Leaf-like carbon nanotube-graphene nanoribbon hybrid reinforcements for enhanced load transfer in copper matrix composites

Ming Yang[1], Lin Weng[1], Hanxing Zhu[2], Fan Zhang[1], Tongxiang Fan[1], Di Zhang[1]*

[1]State Key Laboratory of Metal Matrix Composites, Shanghai Jiao Tong University, 800 Dongchuan Road, Shanghai 200240, P. R. China

[2]School of Engineering, Cardiff University, Cardiff CF24 3AA, UK

*Corresponding author. Tel: +86-21-54747779. E-mail: txfan@sjtu.edu.cn (Tongxiang Fan)

Abstract

A leaf-inspired nanoengineering is employed for the structural design of carbon nanofillers. We fabricate leaf-like carbon nanotube (**CNT**)-graphene nanoribbon (**GNR**) hybrids as novel reinforcements for a copper matrix composite. The straight and stiff CNT 'midribs' are conducive to individual dispersion while the two-dimensional GNR 'margins' provide more sufficient interface contact area and deformation gradient zone, giving rise to significantly improved interfacial stress transfer and mechanical strength as compared to the unmodified nanotubes. The mechanics and strengthening mechanism are further rationalized by finite element analysis and the generalized shear-lag theory.

Key words: metal matrix composites, CNT-graphene hybrids, bio-inspired, shear-lag, finite element analysis

Carbon nanotubes (**CNT**s) have attracted considerable attention as composite enhancers in the past two decades, owing to their extraordinary one-dimensional (**1D**) sp^2-bonding nanostructure and fascinating physi-chemical properties. Specifically, despite constant progress in the field of CNT-reinforced metal matrix composites (**MMC**s), the reinforcing efficiency is still notably lower than the theoretically predicted result [1, 2]. This has been attributed to the agglomeration and non-uniform dispersion of CNTs, the poor cohesion strength and negligible load-transfer at the metal-inorganic interface, as well as the damage of CNTs during processing. In this regard, various kinds of techniques, including friction stir processing [3], high energy ball milling [4], *in-situ* grown [5], flake powder metallurgy [6-8], solution mixing [9], molecular level mixing [10], interfacial modification [11] and so forth, have been developed to address the CNT aggregation and improve the interfacial conditions between CNT and metals. However, little attention has been paid to investigating the effect of structural modification of multi-walled CNTs (**MWCNTs**), and the ensuing interfacial and mechanical responses still remain unclear.

Notably, when serving as nanofillers, their size, dimension and geometry substantially determine the interfacial configuration, load-transfer characteristic and consequently the overall mechanical performance of composites at the macroscale [12, 13]. For example, Alivisatos *et.al* [14] have reported that branched nanofillers have the potential for optimization of nanocomposite Young's modulus over their linear counterparts. In the case of CNT-reinforced MMCs, because of poor mechanical interlocking and easy interfacial sliding between nanotubes and the matrix, the pull-out mode is the dominant failure mechanism,

significantly limiting the reinforcement role [8, 15, 16]. In addition, the exceptional strength of nested inner graphene cylinders in MWCNTs is barely exploited because the extremely weak inter-wall shear resistance allows only the defective outermost walls to carry the load [17]. In fact, MWCNTs are inherently composed of nested and curled graphene layers. Therefore, it is feasible to *in-situ* fabricate inter-connected CNT-graphene hybrids to improve the metal-nanocarbon interfacial shearing and the load-bearing ability of CNT walls.

Plant leaves, typically consisting of a robust midrib and planar leaf laminas (**Fig. 1**a), are elegantly evolved to be strong enough to suffer from external damages owing to their structural coupling effect. Inspired by the configuration of plant leaves, here we report a structural design of carbon nanofillers, in which the middle nanotube and the graphene nanoribbon (**GNR**) wings are inter-welded by carbon sp^2-bonding for synergistically enhancing the load-transfer efficiency and mechanical properties of **MMC**s. Mass leaf-like CNT-GNR hybrids (denoted as **LCGH**s) are synthesized through well controlled unzipping of the outermost layers of MWCNTs. Herein, the inherent CNT midribs serve as a strong and stiff framework to avoid GNR coagulation, whilst the exfoliated GNR parts provide high surface area and abundant hydrophilic oxygenated groups that can introduce more robust interfaces for carrying load as well as facilitating their dispersion in solvents. We achieve an substantial enhancement of load-transfer efficiency and the ensuing boost of mechanical strength in copper matrix composites infused with individually embedded LCGHs (designed as **Cu/LCGH**s) as compared to those reinforced with unmodified CNTs (**Cu/UCNT**s), which highlights the effect of this customization of carbon nanostructure. The mechanics and strengthening mechanism are further rationalized by generalized shear-lag theory and finite element analysis, which suggests

that the strong interfacial bonding, optimized orientation control and especially the unique geometric factors of the novel hybrid reinforcement are conducive to a more effective capability for transmitting stress from Cu matrix.

Bulk LCGHs were firstly prepared by mimicking the typical midrib-margin structure of *Saccharum officinarum Linn* leaves (**Fig. 1**a) through chemical unzipping of several outer-layers of MWCNTs by the conventional Hummers method [18], as illustrated by the schematic showing of Fig. 1b. Herein, the few-layered GNRs, exfoliated from the MWCNTs and extended seamlessly from the perimeter of an individual CNT, are like a leaf laminas, whilst the intact nanotube is similar to a leaf midrib. This configuration change is unambiguously proved by transmission electron microscope (**TEM**, JEM-2100F, JEOL) images (Fig. 1c-d), scanning electron microscope (**SEM**, S-4800, Hitachi) image (Fig. 1e) as well as the atomic force microscope (**AFM**, MultiMode-8, Bruker) topography (Fig. 1f). The well-defined selected area electron diffraction (**SAED**) pattern (Fig. 1d inset) shows elongated diffraction rings along the tube axis, which suggests a retention of crystalline structure and inherent nanotube of LCGHs [19]. Moreover, AFM height profile (Fig. 1f inset) also demonstrates a CNT core of ~100nm thick coupling with side GNR wings of several nanometers thick (<10 layers).

A wet-fusing assembly approach (namely, the hetero-aggregation method [9, 12]), which enables quick assembly, clean interface and scalable preparation, was adopted to obtain homogenously mixed copper-nanofiller hybrid powders. LCGHs are well-dispersed in solvents because they are enriched with negatively charged, hydrophilic moieties (carboxyl, hydroxyl and epoxy groups) after chemical oxidation, as verified by X-ray photoelectron spectroscopy (**XPS**, AXIS UltraDLD, Kratos) profile (**Fig. 2**a) and Fourier transform infrared (**FTIR**,

Nicolet 6700, ThermoFisher) spectra (**Fig. S1**) [19]. The stiff and straight midribs are also conducive to the dispersion of individual LCGHs, because the GNR parts are prone to aggregate due to strong van der Waals interactions and the large surface area [18]. Concurrently, Cu powders with an average diameter of 0.2-2.0 um have positive charge on the surface when dispersed in ethanol solution [9]. As a result, when the two suspensions are co-blended, a large number of Cu powders are available to arrest, sandwich and anchor individual LCGHs through electrostatic force adsorption, giving rise to well-dispersed LCGHs inside the co-deposits (Fig. 2b). The hybrid powders were easily collected and then consolidated and transformed into a fully dense, macroscopic bulk by spark plasma sintering (**SPS**) and large-strain hot rolling (ε=1.97). Meanwhile, lengthwise rotation of LCGHs occurred in the copper matrix during these heavy co-deformations, which otherwise leads to LCGH realigning along the rolling direction (**RD**), as shown in Fig. 2c. Cu/UCNTs that have almost identical microstructure with Cu/LCGHs were also prepared as reference materials, using the same processing conditions, and the details of the fabrication procedure, material characterization and test are provided in the supplementary material.

Mechanical strength data of Cu/LCGHs, Cu/UCNTs and unreinforced Cu matrix obtained from tensile tests are summarized in Fig. 2d, **Fig. S2** and **Table S1**. Cu/LCGHs clearly outperform Cu/UCNTs for improving the tensile strength of Cu matrix (an increase of 39.1~130% and 31~97.3%, respectively). The strength of MMCs has been described on the basis of a simplified shear-lag model, according to which the applied load is transferred to carbon nanofillers through shear stress developed in the compliant metal matrix [7, 15]:

$$\sigma_c = \alpha V_f \sigma_f + (1 - V_f)\sigma_m$$

$$\alpha = 1 - \frac{\sigma_f}{\tau_m s} \text{ for } s > s_c,\ \alpha = \frac{\tau_m s}{\sigma_f} \text{ for } s < s_c$$

where σ_f, V_f, s are the tensile strength, volume fraction and aspect ratio of the reinforcement, respectively; τ_m is the matrix shear yield strength (58 MPa), s_c is the critical aspect ratio given by $s_c = \frac{\sigma_f}{2\tau_m} = 86.2$. A comparison of the relative strength of composite to matrix ($\boldsymbol{\sigma_f/\sigma_m}$) with those expected from the shear-lag model demonstrates that the strength data of Cu/UCNTs agree well with the theoretical predictions, whilst the σ_f/σ_m values of Cu/LCGHs are well above the predicted curve. This verifies the conjecture that the leaf-like nanofillers are substantially more distinguished than pristine CNTs for reinforcing metals.

The superior strengthening capability is further illustrated by isolating the load-bearing effects of LCGHs and UCNTs. The strength increase of nanocarbon reinforced MMCs is generally ascribed to a synergy of Hall-Petch strengthening ($\boldsymbol{\Delta\sigma_{H-P}}$), load-transfer effect ($\boldsymbol{\Delta\sigma_{L-T}}$), geometrically necessary dislocation strengthening ($\boldsymbol{\Delta\sigma_{GND}}$), and Orowan strengthening ($\boldsymbol{\Delta\sigma_{Orowan}}$) [12, 16, 20]. In detail, $\Delta\sigma_{H-P} = kD^{-1/2}$, where k is a material constant and D the mean grain size; $\Delta\sigma_{Orowan} = \frac{0.4MGb}{\pi\lambda(1-\upsilon)^{1/2}} \ln\left(\frac{\pi\gamma_s}{4b}\right)$, where Taylor factor M = 3.06, shear modulus G = 42.1GPa, Poisson's ratio $\upsilon = 0.355$, Burgers vector b = 0.256nm, effective reinforcement particle diameter $\gamma_s = \sqrt[3]{\frac{3d^2 l}{16}}$, and effective planar inter-particle spacing $\lambda = \gamma_s(\sqrt{\frac{\pi}{4V_f}} - 1)$; $\Delta\sigma_{GND} = \alpha Gb\sqrt{\frac{8V_f\varepsilon_y}{b\gamma_s} + \frac{12V_f\Delta CTE\,\Delta T}{b(1-V_f)\gamma_s}}$, where the constant α = 1.25, ε_y is the yielding strain (0.2%), ΔCTE is the coefficient of thermal expansion (**CTE**) mismatch between nanocarbon and Cu, and ΔT is the maximum temperature change during thermomechanical processing; $\Delta\sigma_{L-T}$ is equal to $\sigma_c - \sigma_m - \Delta\sigma_{GND} - \Delta\sigma_{Orowan} - \Delta\sigma_{H-P}$. Accordingly, the load-transfer efficiency ($\boldsymbol{\delta_{L-T}}$), defined as $\delta_{L-T} = \frac{\Delta\sigma_{L-T}}{(\sigma_c-\sigma_m)V_f}$, is evaluated to be 15.2~57.2 for LCGHs. This value accounts for at least 39% more efficient than that of

UCNTs (ranging from 9.2 to 41.2) as load-bearing units for the MMCs with the same nanophase volume fraction (Fig.2e).

TEM (**Fig. 3**a) and HRTEM (Fig. 3b) images show the distribution and interfacial condition of LCGHs in the metal environment, involving a high density of misfit dislocations generated in the vicinity of Cu-LCGH interface. Herein, the contributions of dislocation-related strengthening factors, *i.e.*, $\Delta\sigma_{GND}$ and $\Delta\sigma_{Orowan}$, play an identical role in reinforcing Cu/LCGHs and Cu/UCNTs. Beside the above mentioned strengthening factors, the distribution and orientation of nanofillers, interfacial condition as well as the texture effect [21, 22] are also known to strongly affect the strengthening role of nanofillers:

i) The lateral 2D nanoribbons exhibit high in-plane rigidity and large out-of-plane flexibility, thereby their strengthening efficiencies are strongly affected by the way individual nanofillers are arranged in composites [6]. SEM and TEM images show that both well-dispersed LCGHs and UCNTs are in parallel with the loading axis, as a result of nanofiller realigning to the RD after large-extent deformation. With these respects, the load-transfer between LCGHs and Cu matrix and the strengthening capability of LCGHs could be fully exerted when applying a load along the direction of their maximum performance.

ii) Interfacial bonding is crucial in composites because it determines the stress-transfer and energy-exchange efficiency between reinforcement and matrix [13]. TEM imaging also indicates highly compact interfaces free of impurities, voids, or gaps (Fig. 3b). Moreover, the existence of native oxygen in LCGHs facilitates the formation of a strong oxygen mediated Cu-O-C covalent bonding, which further promotes the interfacial adhesion [10, 12]. The aforementioned are prerequisite conditions for prominent stress-bearing ability of

reinforcements in metal environment.

iii) Furthermore, EBSD maps (Fig. 3c-d) reflect approximately the same microstructure characteristics of Cu/LCGH and Cu/UCNT composites in terms of texture component (Brass-type {110} <112> for both [22]) and grain size distribution. Hence, by excluding the nanophase distribution, interfacial condition, texture effect and the strengthening factors of $\Delta\sigma_{H-P}$, $\Delta\sigma_{GND}$ and $\Delta\sigma_{Orowan}$, we conclude that the exceptional strength of Cu/LCGHs compared to Cu/UCNTs should be originated from the contribution of load-transfer strengthening only, as a consequence of imparting leaf-like GNRs to pristine nanotubes.

Numerical simulations were further performed using finite-element methods (**FEM**) software (ABAQUS) to quantify and clarify the structural coupling effect on the stress distribution, load-carrying of LCGHs and the overall mechanical response of the bulk composites. As illustrated in **Fig. 4**a, there exists a von Mises stress gradient along either the longitudinal or transverse directions of LCGHs. In addition, the stress amplitude on the attached graphene planes is ~8% larger than that on the middle nanotube. When a tensile load is applied, the interfacial shearing stress transfer preferentially occurs in the side GNRs whereas the CNT midrib plays a less important load-bearing role. Nevertheless, a ~10% more distinguished stress distribution is detected on the midrib of LCGHs than that on the bare UCNTs (Fig. 4b). Nitrogen adsorption-desorption measurements (**Fig. S3**) reveal a 6.67-folds increase of BET specific surface area (255.5 m^2 g^{-1} and 33.3 m^2 g^{-1} for LCNTs and UCNTs, respectively), owing to the unzipping of nanotube outer-walls. Thereby, it is distinguished that the hybrid reinforcement enables a more prominent energy consumption (defined as $\oiint \sigma ds$) during the composite deformation, arising from its ability to optimize the function of the

flexible GNR lamellas for stress transfer and load-carrying associated with the robust part of CNT core. The anchored GNRs may act as 'soft' parts during tensile deformation due to their 2D geometry with a thickness of several nanometers, whereas the CNT core can substantially serve as a 'stiff' part because of its linear shape and considerable diameter. In this manner, an obvious deformation gradient zone and an elevated stress distribution are triggered over the whole CNT-GNR hybrid, which is critically beneficial for interfacial shearing and load transfer from the matrix. Unlikely, their tubular counterpart is typically limited by their smooth and linear shape, which eventually leads to insufficient interfacial contact area, mechanical interlock and energy exchange with Cu matrix.

The optimized load-transfer performance of Cu/LCGHs over Cu/UCNTs is further confirmed by the fractography and facture behavior. The fracture surface of Cu/LCGHs reveals a telescopic fracture of LCGHs inside the ductile dimples (Fig. 4c-d). At variance, the fracture topography of Cu/UCNTs indicates interface debonding and predominant pull-out of intact CNTs (Fig. 4e) [15], given that the aspect ratio of nanofillers is smaller than the critical value S_c here. Therefore, the transition of the operative failure mode from the ineffective pull-out to a dominant telescopic fracture, as illustrated by the schematic showing of Fig. 4f-g, provides direct and compelling evidence for more distinguished load-transfer strengthening contribution of LCGHs than UCNTs [23]. As suggested by the FEM simulations, the application of nanostructural modification contributes to a simultaneous exploitation of the geometrical advantages of both CNTs and GNRs, which maximizes the reinforcing capability of 1D nanotubes and 2D nanobelts. Both the inner CNT core and the inter-welded GNR wings are tore and broken, which implies synergistic reactions upon an applied load accompanied with a

delay of the onset of interfacial slippage and CNT pull-out.

In conclusion, we have presented a bio-inspired configuration design of carbon nanofillers *via* partial unzipping of the outer-layers of MWCNTs to form leaf-like GNR-CNT hybrids, which offers an avenue to modulate the load-transfer and mechanical behavior of MMCs. We have established comprehensive relationships among load-transfer characteristics, failure mechanism and mechanical behavior as a result of this customization of carbon nanostructure. The leaf-like configuration renders LCGHs with a better load-sharing efficiency and reinforcing capacity than their unmodified counterpart, which is rationalized by the generalized shear-lag theory and FEM simulations. The exceptional mechanical response enabled by this strategy may provide guidance for the design of nanocomposites with optimized mechanical properties for a variety of structural applications.

References

[1] S.C. Tjong, Mater. Sci. Eng. R 74(10) (2013) 281-350.

[2] S.R. Bakshi, D. Lahiri, A. Agarwal, Int. Mater. Rev. 55(1) (2010) 41-64.

[3] Z.Y. Liu, B.L. Xiao, W.G. Wang, Z.Y. Ma, Carbon 50(5) (2012) 1843-1852.

[4] H. Li, A. Misra, Z. Horita, C.C. Koch, N.A. Mara, P.O. Dickerson, Y. Zhu, Appl. Phys. Lett. 95(7) (2009) 071907.

[5] C. He, N. Zhao, C. Shi, X. Du, J. Li, H. Li, Q. Cui, Adv. Mater. 19(8) (2007) 1128-1132.

[6] L. Jiang, Z. Li, G. Fan, L. Cao, D. Zhang, Carbon 50(5) (2012) 1993-1998.

[7] Z. Li, G. Fan, Q. Guo, Z. Li, Y. Su, D. Zhang, Carbon 95 (2015) 419-427.

[8] B. Chen, K. Kondoh, H. Imai, J. Umeda, M. Takahashi, Scr. Mater. 113 (2016) 158-162.

[9] S. Cho, K. Kikuchi, A. Kawasaki, Acta Mater. 60(2) (2012) 726-736.

[10] S.I. Cha, K.T. Kim, S.N. Arshad, C.B. Mo, S.H. Hong, Adv. Mater. 17(11) (2005) 1377-1381.

[11] I. Jo, S. Cho, H. Kim, B.M. Jung, S.-K. Lee, S.-B. Lee, Scr. Mater. 112 (2016) 87-91.

[12] M. Yang, L. Weng, H. Zhu, T. Fan, D. Zhang, Carbon 118 (2017) 250-260.

[13] U. Ramamurty, Compos. Sci. Technol. 65(11-12) (2005) 1815-1825.

[14] S.N. Raja, A.C. Olson, A. Limaye, K. Thorkelsson, A. Luong, L. Lin, R.O. Ritchie, T. Xu, A.P. Alivisatos, Proc. Natl. Acad. Sci. U.S.A. 112(21) (2015) 6533-8.

[15] W. Zhou, G. Yamamoto, Y. Fan, H. Kwon, T. Hashida, A. Kawasaki, Carbon 106 (2016) 37-47.

[16] J.G. Park, D.H. Keum, Y.H. Lee, Carbon 95 (2015) 690-698.

[17] M. Estili, A. Kawasaki, Adv. Mater. 22(5) (2010) 607-10.

[18] Z. Guo, J. Wang, F. Wang, D. Zhou, Y. Xia, Y. Wang, Adv. Funct. Mater. 23(38) (2013) 4840-4846.

[19] M. Yang, L. Hu, X. Tang, H. Zhang, H. Zhu, T. Fan, D. Zhang, Carbon 110 (2016) 480-489.

[20] L. Jiang, H. Yang, J.K. Yee, X. Mo, T. Topping, E.J. Lavernia, J.M. Schoenung, Acta Mater. 103 (2016) 128-140.

[21] R.T. Ott, J. Geng, M.F. Besser, M.J. Kramer, Y.M. Wang, E.S. Park, R. LeSar, A.H. King, Acta Mater. 96 (2015) 378-389.

[22] T. Leffers, R.K. Ray, Prog. Mater. Sci. 54(3) (2009) 351-396.

[23] A.J. Kessman, J. Zhang, S. Vasudevan, J. Lou, B.W. Sheldon, Adv. Mater. Inter. 2(2) (2015) 1400110.

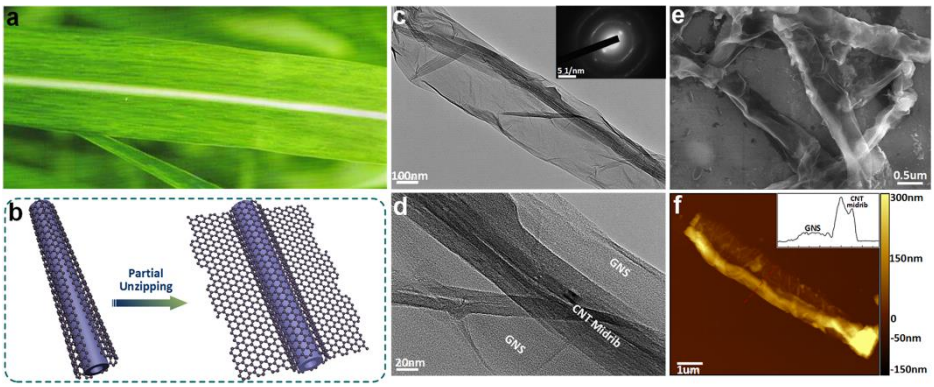

Fig. 1. (a) Photograph of *Saccharum officinarum Linn* leaves showing typical midrib-margin structure. (b) Schematic illustration for the development of LCGHs inspired by leaf structure. (c-d) TEM and HR-TEM images of LCGHs, inset is the corresponding SAED pattern. (e) SEM image of LCGHs. (f) AFM topography of a single LCGH, inset is the corresponding height profile.

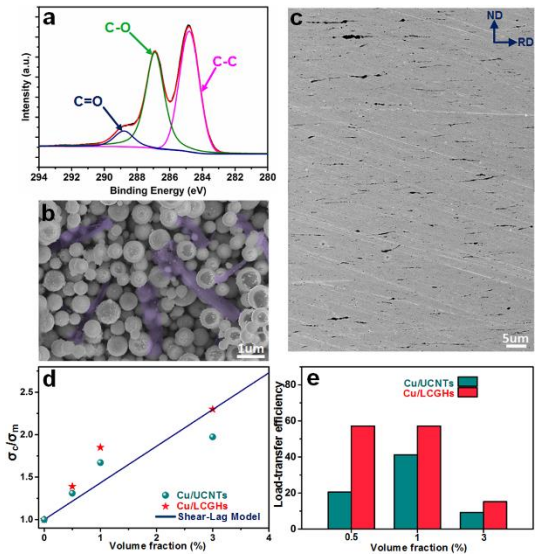

Fig. 2. (a) Deconvoluted XPS C1s spectrum of LCGHs. (b) SEM image displaying homogenously mixed Cu/LCGH hybrid powders. (c) SEM image proving well-embedded, uniformly-distributed and RD-aligned LCGHs in the Cu matrix. (d) σ_f/σ_m values of Cu/LCGHs and Cu/UCNTs, plotted against the volume fraction. These data are compared to theoretical predictions from the shear-lag model (solid line). (e) Load-transfer efficiency of Cu/LCGHs and Cu/UCNTs.

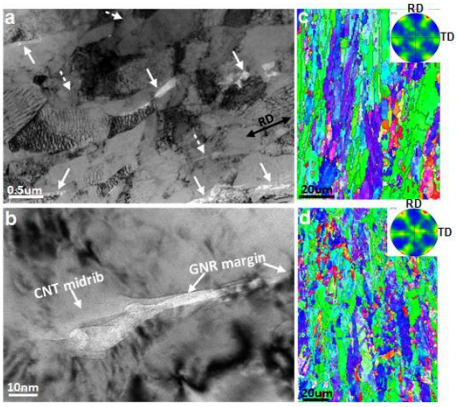

Fig. 3. (a) TEM and (b) HR-TEM images show the distribution and configuration of LCGHs in Cu matrix. The solid lines represent CNT midribs, whereas the dash lines exhibit the GNR margins. (c-d) EBSD maps of Cu/LCGHs and Cu/LCNTs, respectively. Insets are the corresponding {111} pole figures.

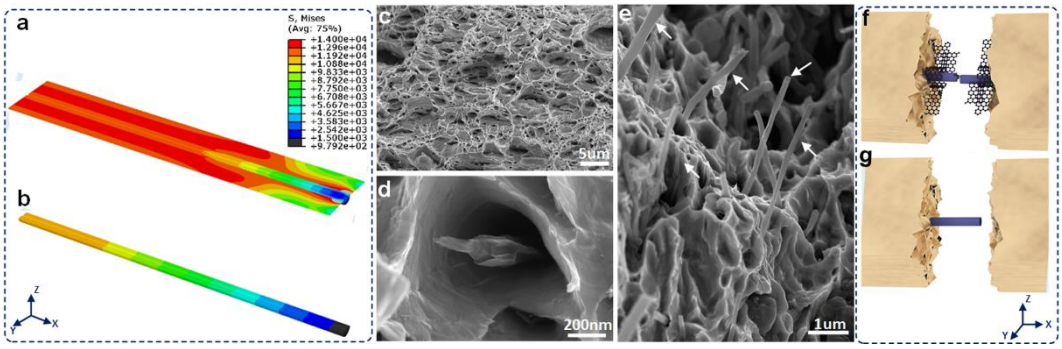

Fig. 4. (a-b) FEM analysis showing the von Mises stress distribution in LCGHs and UCNTs, respectively. The tensile strain is 5%, and the loading direction is in parallel to the X axis. Half of the nanofiller models are displayed. (c) SEM image showing the ductile fracture morphology of Cu/LCGHs. (d-e) HR-SEM images display GNR tearing and CNT midrib breaking of LCGHs, and intact UCNTs pulling out from the matrix, respectively. (f-g) Schematic illustration showing representative nanophase failure types of LCGHs and UCNTs, respectively.